Microfluid Nanofluid (2005) 1: 177–182
DOI 10.1007/s10404-004-0026-3

RESEARCH PAPER

Jung-Yeul Jung · Ki-Taek Byun · Ho-Young Kwak

# Proteinaceous bubble and nanoparticle flows in microchannels

Received: 20 July 2004 / Accepted: 20 September 2004 / Published online: 2 December 2004


**Abstract** Proteinaceous bubbles of 185 nm average diameter were synthesized by a sonochemical treatment of bovine serum albumin (BSA) in an aqueous solution and the nanoparticles ($TiO_2$) solution was made by ultrasonic irradiation. To study the macroscopic flow behavior associated with the changes in the state of the microparticles, a flow test of these solutions in microchannels was done. Also, the size distributions of the proteinaceous bubbles in solution before and after the flow test were measured by a light scattering method. Test results show that the air-filled proteinaceous bubbles in solution adjust their size to reduce the shear stress encountered in the flow through the microchannel. On the other hand, the mass flow rate of the solution with nanoparticle suspensions becomes smaller than that of deionized water in a microchannel of dimension 100×100 $\mu m^2$.

**Keywords** Bovine serum albumin · Light scattering method · Microchannel · Nanoparticle · Proteinaceous bubble

## 1 Introduction

Understanding the characteristics of the flow of particle suspensions in a microchannel is very important in designing BioMEMS devices and in biomedical research. Especially, the flow of biological particles, such as vesicles, which have found diverse and important practical applications ranging from microencapsulation of dyes to drug delivery systems, should be studied to understand the flow behavior associated with these particles in a microchannel (Tay 2002).

In this study, proteinaceous microbubbles, a type of vesicle, were synthesized by ultrasonic radiation of bovine serum albumin (BSA) in an aqueous solution below the sonoluminescence condition, where the center temperature of the transient bubble at the collapse exceeds 5,000 K (Suslick et al. 1986). The average diameter of the synthesized proteinaceous bubbles having a log-normal distribution is about 185 nm. Microchannels connecting two reservoirs were fabricated on a silicon wafer, whose specification is (100) orientation, p-type, and 525 ± 5-μm thickness, to test the flow of biological particles and nanoparticle suspensions. The dimensions of the microchannels used in this study were 200×100, 150×100, and 100×100 $\mu m^2$ cross section, and the channels have the same length of 15 mm.

To investigate the characteristics of the flow of fluid containing the proteinaceous bubbles and nanoparticles of $TiO_2$ having size 20–50 nm in the microchannels fabricated, the volume flow rates of the flow of the proteinaceous bubbles and $TiO_2$ particle suspensions were measured and compared with the case of the flow of deionized water. Also, the size distribution of the proteinaceous bubbles before and after the flow tests were measured by a light scattering method to understand the mechanics of microchannel flow where the particles are under nonuniform shear and compression on the biological particles (Babcock et al. 2000).

The mass flow rates of the fluid with the nanoparticle suspensions are lower than the case of pure water for various driving pressures tested. After the proteinaceous bubbles in aqueous solution experiencing flow through the microchannel, the average diameter of the bubbles becomes smaller, even though the shape of the bubbles is unchanged. The average diameter of the proteinaceous bubble becomes more smaller at a lower flow rate of 2.02 $cm^3$/min or at a higher flow rate of 6.20 $cm^3$/min in the 150-μm width channel.

J.-Y. Jung · K.-T. Byun · H.-Y. Kwak (✉)
Mechanical Engineering Department,
Chung-Ang University,
Seoul, 156-756, Korea
E-mail: kwakhy@cau.ac.kr
Fax: +82-2-8267464

## 2 Sonoluminescence system

### 2.1 Sonoluminescence phenomena

Sonoluminescence is the phenomenon of light emission associated with the catastrophic collapse of a microgas bubble under ultrasound excitation (Gaitan et al. 1992). The light emission from a well controlled single bubble under ultrasound is found to be characterized by pico-second flashes of a continuous spectrum with no major peaks (Hiller et al. 1992, 1998; Gompf et al. 1997). Hydrodynamic solutions for the oscillating gas bubble yielded a gas temperature range of 10,000–30,000 K and a pressure of 10,000 bar at the collapse (Kwak and Yang 1995; Kwak and Na 1996, 1997), at which, the bubble wall acceleration exceeds $10^{12}$ m/s$^2$ (Kwak and Na 1996; Weninger et al. 1997). Consequently, the bubble collapse produces a liquid zone at a high temperature of 1,000°C and a pressure of 500 bar (Kwak and Na 1995), where high energy chemical reactions can be made (Suslick 1990).

Rather than a single bubble, a lot of transient bubbles can be generated by the irradiation of high-intensity ultrasound into an aqueous solution. The collapse of clouds of bubbles accompanying light emission (MBSL; multibubble sonoluminescence) also produces intense local heating and high pressure, which makes it possible to synthesize proteinaceous microbubbles (Grinstaff and Suslick 1991). The nucleated gas bubbles, by the irradiation of ultrasound to the solution, may be stabilized by the chemical cross-linking of the protein molecules at the interface (Grinstaff and Suslick 1991). Such an elastic layer can be made by the oxidization of the cysteine residues of protein by superoxide, created due to the extremely high temperature inside the gas bubble.

### 2.2 Experimental apparatus for sonoluminescence

The experimental apparatus for MBSL consists of a cylindrical quartz cell into which a 5-mm diameter titanium horn (Misonix XL2020, USA) is inserted, as shown in Fig. 1. An o-ring at the top of the cell provides a seal between the horn and the cell. The cell has three ports; one is for a temperature sensor and the others are for the input and output of air. Continuous circulation of water to the bath in which the cell is immersed keeps the temperature of the solution inside the cell around 50°C. The sonoluminescence condition can be found at the proper ultrasound intensity, in terms of the liquid temperature and the distance between the titanium horn and the bottom of the cell, by trial and error. The emission of blue light around the horn tip by the air bubble cloud in water at 3°C is shown in Fig. 2. Proteinaceous bubbles were synthesized by the irradiation of an aqueous solution of 5∼10% (wt/vol) BSA with ultrasound below the sonoluminescence condition.

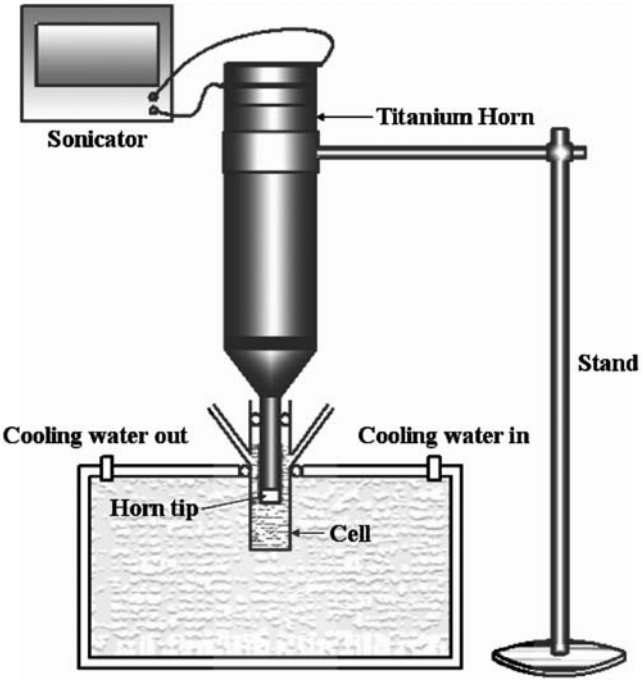


**Fig. 1** An experimental setup to synthesize proteinaceous bubbles

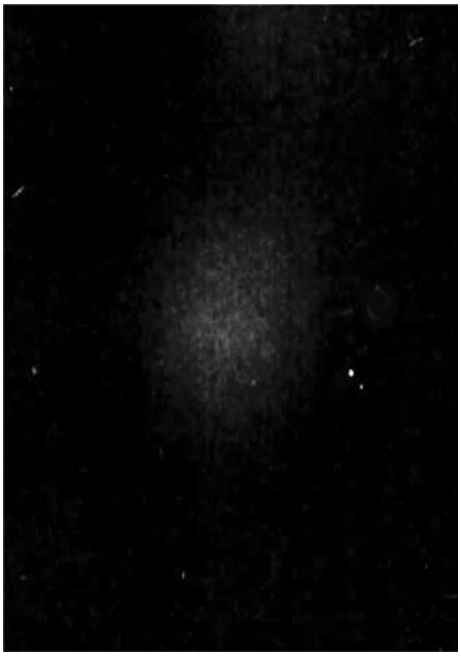

**Fig. 2** Blue light emitted by the air bubble cloud in water at the sonoluminescence condition

## 3 Microchannel system

### 3.1 Device design and fabrication

A silicon wafer polished on both sides (p-type (100) orientation single crystal with $525 \pm 5$ μm thickness) was

used to fabricate an integrated microsystem consisting of five microchannels on one side. A 20×30-mm die for the device was used. On the back side of the wafer, an oxide layer was also formed and patterned to serve as an etch mask for plasma etching, which produced a 100-μm deep flow channel with a rectangular cross section. The microchannels were etched using a Bosch process with the aid of inductive-coupled plasma. Such an etching process yielded a wavy pattern of the vertical surface with a surface roughness of 0.15∼0.17 μm. The main fabrication steps described above are shown schematically in Fig. 3. After these processes were completed, a pyrex-7740 glass wafer (thickness 525 μm) having two holes as inlet and outlet ports of the liquid was anodically bonded to the back side of the silicon substrate to cover the fluid manifolds and microchannels. The fabricated microchannels were 100, 150, and 200-μm wide, respectively, all were 100-μm high, and 15-mm long. The manifolds were 500-μm wide, 9-mm long, and 100-μm deep. A schematic of the complete device with dimensions in millimeters is shown in Fig. 4.

### 3.2 Experimental apparatus for microchannel flow

A schematic of the experimental apparatus used is shown in Fig. 5. The apparatus consists of: (1) a working fluid handling system; (2) the microchannel test chip; and (3) a data acquisition system. The working fluid handling system includes a high-pressure gas source, a pressurized fluid reservoir, a microfilter, a pressure gauge, and a volumetric graduated cylinder. Deionized water, aqueous solutions with nanoparticle and with proteinaceous bubble suspensions were used as the working fluids. The working fluids were driven by a high-pressure argon gas, and the driving pressure was adjusted by a pressure regulator. The liquid was freely discharged from the outlet manifold so that the outlet pressure would be atmospheric. The mass flow rate of the working fluid was obtained by measuring the liquid mass flowed through the graduated cylinder during

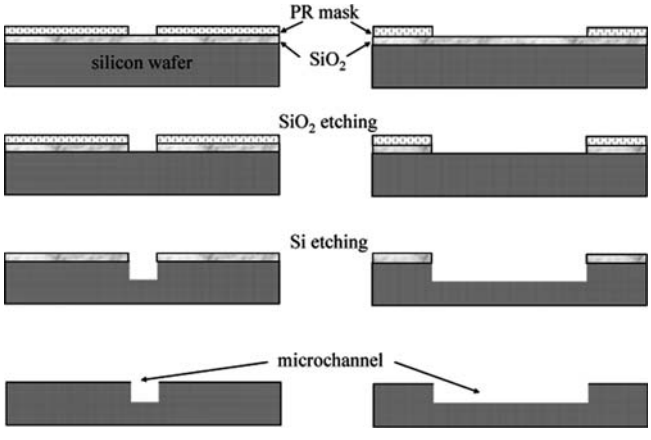


**Fig. 3** Schematic of the fabrication steps for the microchannels

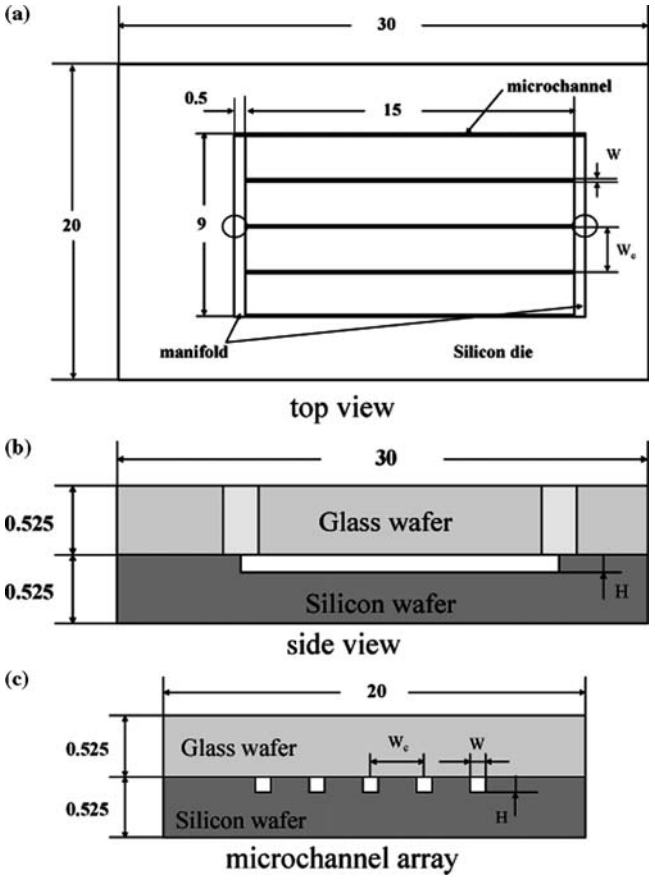


**Fig. 4a–c** Schematic of the fabricated microchannel. **a** Top view. **b** Side view. **c** Microchannel array (dimensions in mm)

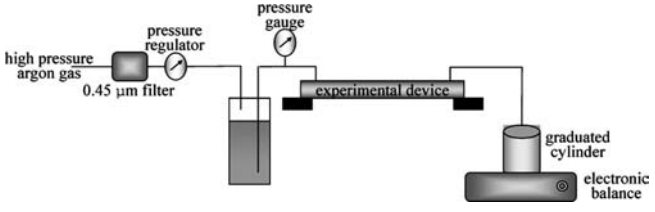


**Fig. 5** Schematic for the experimental test setup

10 min with a electronic balance (Scaltec SBC 31, Germany) having a precision of ±0.001 g. Human error in the measurement of the flow rate is less than 0.5%. A pressure gauge was used to monitor the fluid pressure near the inlet manifold. The working fluids at approximately 21–24°C were fed into the input manifold through the inlet hole at driving pressures of up to 0.30 MPa.

### 3.3 Preparation of a nanofluid

A nanofluid was prepared by mixing $TiO_2$ nanoparticles of size 20∼50 nm in diameter with deionized water by ultrasound irradiation for 10 h or so. The solution contains about 0.1 wt% of $TiO_2$ particles. No aggrega-

tion or precipitation of $TiO_2$ particles in the solution were found, even after 10 days.

## 4 Results and discussion

### 4.1 Synthesis of proteinaceous microbubbles

An electron micrograph by a transmission electron microscope (TEM) for the proteinaceous bubbles synthesized by the irradiation of an aqueous solution of 5% (wt/vol) BSA with ultrasound is shown in Fig. 6. The solution was irradiated with an ultrasound frequency of 20 kHz for 5 min at an acoustic power of 200 W/cm$^2$ and at a solution temperature of 50°C. The diameter of the proteinaceous bubbles whose size distribution is log-normal, as shown in Fig. 7, is about 185 nm. A small number of proteinaceous bubbles greater than 3 μm in size were also found. The bubble size obtained in this experiment is smaller by an order of magnitude to the size of 2.5 μm obtained by Suslick with BSA (Suslick 1998). However, vesicles less than 200 nm in diameter were reported to be useful as a model membrane, as capsules for agents in drug delivery, and as substrates for enzymes and proteins (Kaler et al. 1989). The long-lived stability of the gas bubbles whose sizes are in the range 100∼200 nm in solution may be explained by a varying permeability model by Yount (1982). This size range of bubbles that may have a single bilayer of surface active agent at the interface are small enough to remain in the solution and are strong enough to resist collapse. The proteinaceous bubbles synthesized were found to be stable for months.

### 4.2 Size distribution change of proteinaceous bubbles in a microchannel

The air-filled proteinaceous bubbles, which may be considered as biological particles, may change their shape and size under the elongational and shear flow encountered in the flow through the microfluidic device.

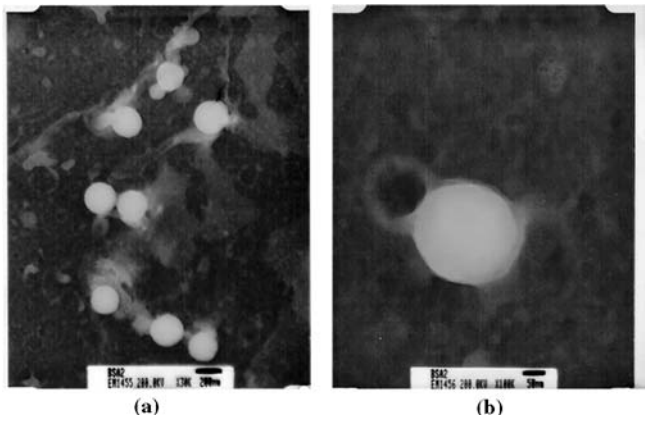


**Fig. 6** **a** Transmission electron micrograph of sonochemically prepared proteinaceous microbubbles from BSA. **b** Enlarged view

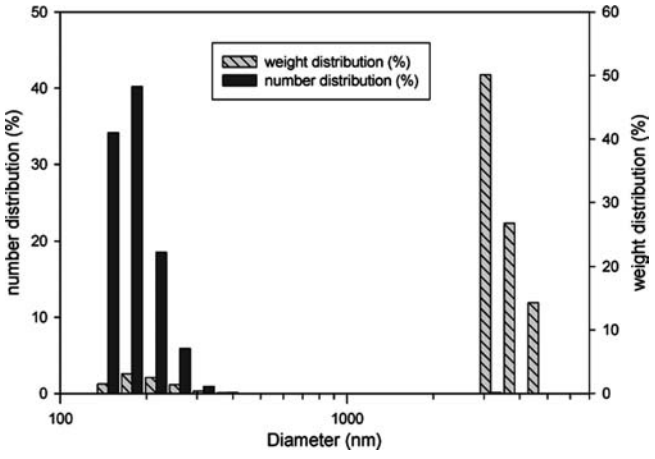


**Fig. 7** Size distributions of proteinaceous bubbles synthesized by sonochemical treatment

Flow tests of such particles in a microchannel may reveal the macroscopic flow behavior associated with changes in the state of nanoparticles in a solution. The size distribution for the proteinaceous bubbles in an aqueous solution before and after the flow test was also measured by light scattering equipment (ELS-8000, Otsuka Electronic, Japan) for the fluid behavior in the microchannel.

Figure 8 shows an electron micrograph by TEM for the bubbles after the flow test in the 150-μm width microchannel. As can be seen from this image, the spherical shape of the bubbles was not changed. However, as shown in Fig. 9a, the size distribution of the bubbles was

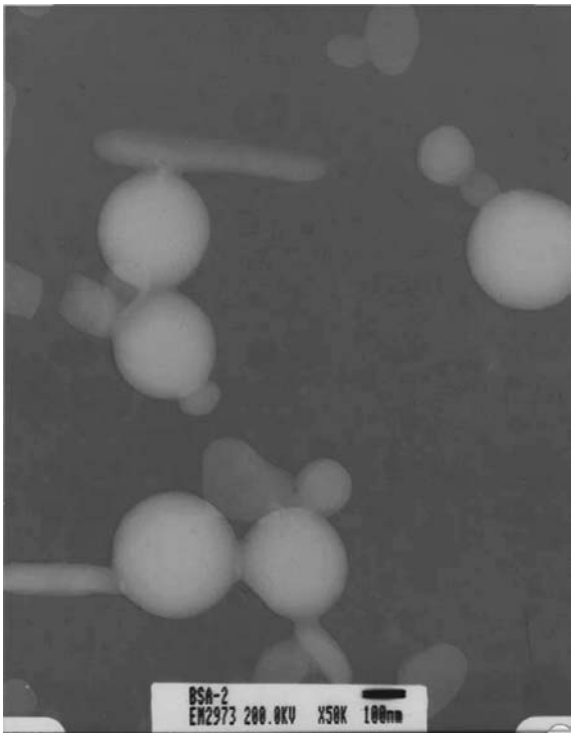


**Fig. 8** Tunneling electron micrograph (TEM) of proteinaceous bubbles after the flow test

changed considerably after the flow test, especially for the flow test in the narrow width microchannel. After the flow test in the 150-μm width channel, the average size of the bubbles reduces to 100∼140 nm from 185 nm at the lower (2.02 $cm^3$/min) and higher (6.20 $cm^3$/min) flow rates tested. At the medium range of the flow rates (3.08∼5.53 $cm^3$/min), the average bubble size reduces to 130 nm. On the other hand, the average size of the bubbles reduces to 135 nm at any of flow rates tested in the 200-μm width channel, as shown in Fig. 9b. The results from the flow test for the solution with proteinaceous bubbles indicate that the shear stress effects reduce the size of the deformable particle significantly, even though the flow rate effect on the change of size distribution is not conclusive.

### 4.3 Flow characteristics of proteinaceous bubbles or nanoparticle suspensions

As shown in Fig. 10, the flow rates of the solution with nanoparticle suspensions are lower than the flow rate of deionized water at various driving pressures tested. The mass flow rate of the solution of $TiO_2$ dispersion is less than that of deionized water by 0.07 g/min. However, the flow rates of the solution with proteinaceous bubbles are almost same as the flow rate of deionized water in an experimental error range up to the driving pressure of 300 kPa. Its deviation is less than ±0.01 g/min. On the other hand, the flow rate of the solution with nanoparticle suspensions reduces appreciably at various driving pressures tested, as shown in Fig. 10, which indicates that the shear stress due to the nanoparticles in the solution affects the velocity distribution near the wall. On the other hand, the air-filled proteinaceous bubbles in the solution adjust their size to reduce the effect of shear stress in the microchannel. As expected, the solid particles in the solution have no ability to adjust their size in the shear flow field. Finally, it is noted that the fluids tested in this experiment show Newtonian viscosity with a dynamic viscosity value of 1.03 cP at 23°C, as shown in Fig. 11.

## 5 Conclusion

To investigate the macroscopic flow behavior associated with the changes in microscopic state, the flow rate of solutions with proteinaceous bubbles, and with nanoparticle suspensions and deionized water were measured. Also the size distributions of the proteinaceous bubbles before and after the flow test were measured by a light scattering method. The proteinaceous bubbles were

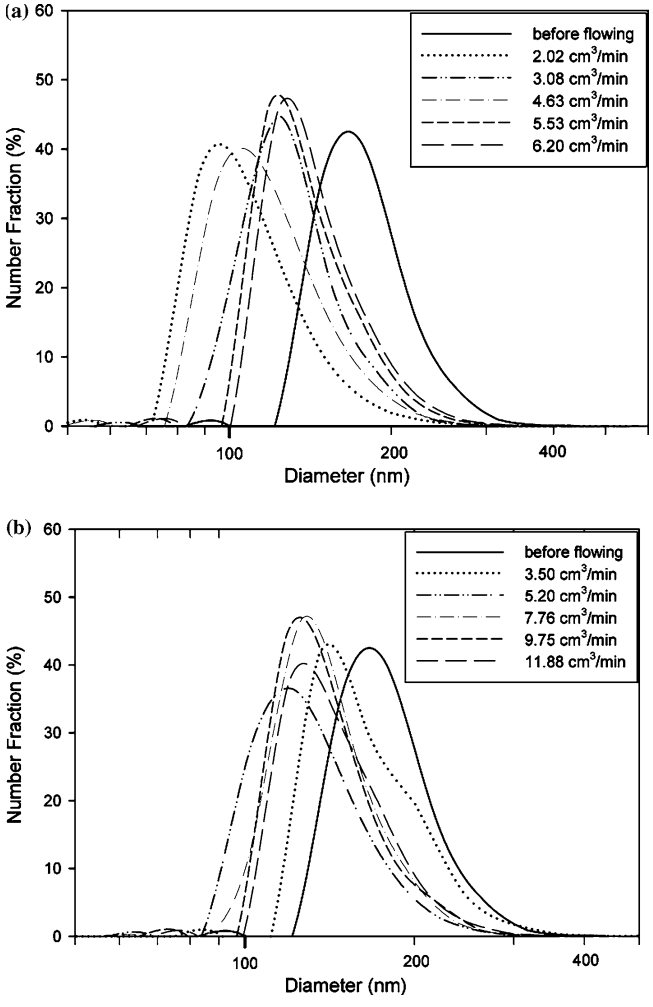


**Fig. 9a, b** Size distribution after the flow test in the 150-μm width (**a**) and 200-μm width (**b**) microchannels

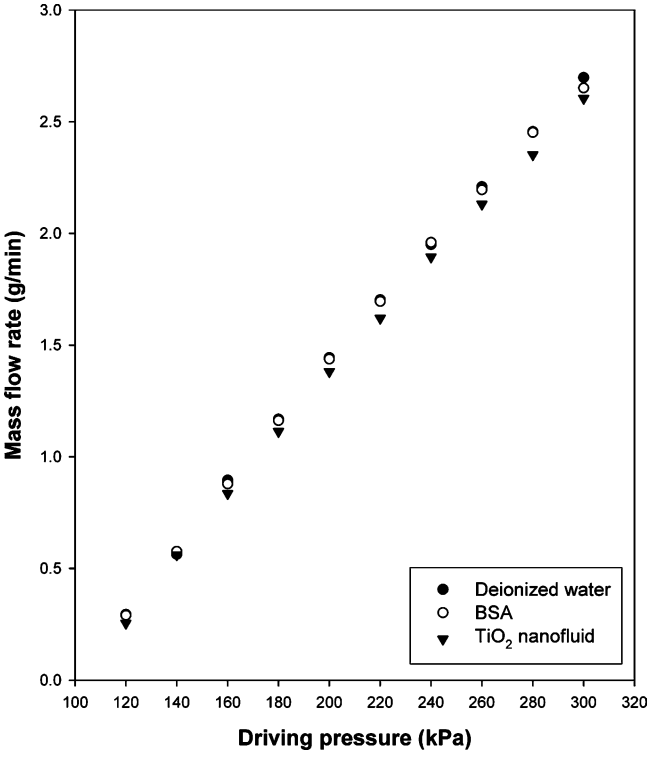


**Fig. 10** Mass flow rates for different driving pressure in the 100-μm width channel

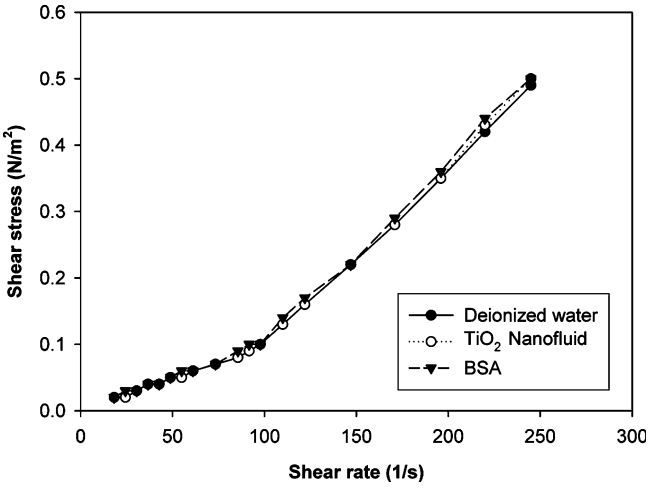


**Fig. 11** Shear stress versus shear rate for the fluids tested

found to adjust their size to reduce the effect of the shear stress without sacrificing the flow rate. However, the mass flow rate of the solution with nanoparticle ($TiO_2$) suspensions becomes appreciably smaller than that of deionized water at various driving pressures tested in the 100μm width microchannel.

**Acknowledgements** This work was supported by the Korea Research Foundation, grant number KRF-2003-041-D00114.

## References

Babcock HP, Smith DE, Hur JS, Shagfeh ESG, Shu S (2000) Relating the microscopic and macroscopic response of a polymeric fluid in a shearing flow. Phys Rev Lett 85(9):2018–2021

Gaitan DF, Crum LA, Church CC, Roy RH (1992) Sonoluminescence and bubble dynamics for a single, stable, cavitation bubble. J Acoust Soc Am 91(6):3166–3183

Gompf B, Gunter R, Nick G, Pecha R, Eisenmenger W (1997) Resolving sonoluminescence pulse width with time-correlated single photon counting. Phys Rev Lett 79(7):1405–1408

Grinstaff MW, Suslick KS (1991) Air-filled proteinaceous microbubbles: synthesis of an echo-contrast agent. Proc Natl Acad Sci USA 88(17):7708–7710

Hiller RA, Putterman SJ, Barber BP (1992) Spectrum of synchronous picosecond sonoluminescence. Phys Rev Lett 69(8):1182–1184

Hiller RA, Putterman SJ, Weninger KR (1998) Time-resolved spectra of sonoluminescence. Phys Rev Lett 80(5):1090–1093

Kaler EW, Murthy AK, Rodriguez BE, Zasadzinski JAN (1989) Spontaneous vesicle formation in aqueous mixtures of single-tailed surfactants. Science 245(4924):1371–1374

Kwak H-Y, Na JH (1996) Hydrodynamic solutions for a sonoluminescing gas bubble. Phys Rev Lett 77(21):4454–4457

Kwak H-Y, Na JH (1997) Physical processes for single bubble sonoluminescence. J Phys Soc Jpn 66(10):3074–3083

Kwak H-Y, Yang H (1995) An aspect of sonoluminescence from hydrodynamic theory. J Phys Soc Jpn 64(6):1980–1992

Suslick KS (1990) Sonochemistry. Science 247(4949):1439–1445

Suslick KS (1998) Sonochemistry. In: Kirk-Orthmer encyclopedia of chemical technology, vol 16, 4th edn. Wiley, New York, pp 517–541

Suslick KS, Hammerton DA, Cline RE (1986) The sonochemical hot spot. J Am Chem Soc 108:5641–5642

Tay EH (2002) Microfluidics and BioMEMS applications. Kluwer, Boston, Massachusetts

Weninger KR, Barber BP, Putterman SJ (1997) Pulsed Mie scattering measurements of the collapse of a sonoluminescing bubble. Phys Rev Lett 78(9):1799–1802

Yount BE (1982) On the evolution, generation, and regeneration of gas cavitation nuclei. J Acoust Soc Am 71(6):1473–1481